Correlation function-based finite-difference time-domain method for simulating ultrashort pulse propagation. I. Formalism

Julie A. Gruetzmacher[a)]
Department of Chemistry, The James Franck Institute and The Institute for Biophysical Dynamics, The University of Chicago, Chicago, Illinois 60637

(Received 1 November 2002; accepted 16 April 2003)

A finite-difference time-domain formalism for simulating coherent linear pulse propagation is presented that incorporates a medium response described by any two-time energy gap correlation function. Two algorithms, for real and complex correlation functions, are developed to evaluate the electric polarization through explicit treatment of the density matrix for a two-level system. The coherence relaxation terms in the resulting finite-differenced Maxwell–Liouville equations depend on integrals over the energy gap fluctuation correlation function. The algorithms are used to simulate ultrashort mid-infrared pulse propagation through optically dense samples of HDO in liquid D_2O as a demonstration of their performance and flexibility. These algorithms represent a first step toward the goal of incorporating complicated material responses into the full-field simulation of nonlinear pulse propagation and nonlinear optical spectroscopy.
[DOI: 10.1063/1.1580804]

I. INTRODUCTION

The study of optical coherence phenomena has a long history, rooted in the seminal work of Brewer and Shoemaker,[1,2] McCall and Hahn,[3] and Hartmann and co-workers,[4,5] among others.[6] These early investigations have developed into modern-day ultrafast nonlinear optical spectroscopy and its theoretical description.[7] Ultrafast spectroscopic techniques can now measure third- and higher-order nonlinearities on femtosecond time scales;[8–11] however, the more simple phenomena of the optical free-induction decay (FID) and coherent pulse propagation still impact nonlinear measurements and are subjects of continuing investigation.[12,13] Pulse propagation effects, i.e., features due to the coherent propagation of short pulses through a resonant medium, contribute to measured optical responses and warrant special attention in time-resolved spectroscopic studies using few-cycle pulses and optically dense samples.[14–20]

One area of ultrafast spectroscopy in which propagation effects are particularly relevant is nonlinear mid-infrared (mid-IR) spectroscopy. The study of nonlinear responses from vibrations is challenging because vibrational transition dipole moments ($\boldsymbol{\mu}$) are typically much smaller, often by orders of magnitude, than those of electronic transitions. The factor of $|\boldsymbol{\mu}|^8$ that appears in expressions for third-order nonlinear signals therefore results in vibrational responses that are significantly smaller than their electronic counterparts. In addition to employing signal averaging techniques to enhance signal to noise ratios, two strategies are often pursued to make such measurements possible: increasing incident pulse energies, sometimes to the level of tens of microjoules, and/or increasing chromophore concentration. It is a technological challenge to maintain short mid-IR pulse durations throughout the multiple parametric generation stages needed to achieve high pulse energies; therefore, the latter approach is often more feasible. High oscillator concentrations are also intrinsic to studies of neat liquids. However, pulses with durations on the order of the inverse linewidth of a transition can become distorted during propagation through highly absorptive samples, a phenomenon resulting from destructive interference between the initial pulse and the FID(s) it drives.[21,22] These "FID beats"[20] on the trailing edge of pulses can distort the resultant waveforms and therefore complicate the retrieval of dynamic information from experimental transients.[18,19,23,24] For example, Spano and Warren have shown that the dephasing time measured via photon echo spectroscopy depends on optical density (OD) when sample ODs are roughly one or higher.[23] While such optical density effects were observed in linear mid-IR pulse propagation decades ago,[25,26] explicit consideration of their influence on nonlinear mid-IR transients has been limited: one report incorporating propagation effects on mid-IR pump-probe measurements has appeared in the literature,[17] and inclusion of propagation effects was briefly mentioned in the analysis of recent photon echo measurements.[27] It is therefore desirable to develop the appropriate machinery to account for such effects in the simulation of signals so that the dynamic time scales of molecular relaxation can be determined accurately. The first step toward realizing this goal is the development of a simulation algorithm for the simplest case—that of linear pulse propagation. Such an algorithm can then form the basis for more complicated extensions to nonlinear responses.

There are a number of strategies for modeling the influence of pulse propagation on optical transients. In the ultrafast spectroscopy literature, the most common method is to model the propagation of the pulse envelope with a set of Maxwell–Bloch equations under the rotating wave

[a)]Electronic mail: jgruetzm@uchicago.edu

(RWA) and slowly-varying envelope (SVEA) approximations.[17–19,23,24,28] While this approach is computationally simple, the RWA and SVEA lose accuracy for transitions whose spectral width is comparable to their center frequency[12] and few-cycle optical pulses, respectively. Furthermore, this method assumes that the Bloch model is an appropriate description of the medium; i.e., the relaxation is purely homogeneous. In addition, any phase information about the field is lost as only the pulse envelope is simulated. Therefore, it would be advantageous to develop a more general method that propagates the full electric field of the pulse and accounts for a possibly non-Markovian response of the material (particularly important for nonlinear extensions) while not relying upon the RWA or SVEA.

This paper presents a computational approach for modeling linear, ultrashort pulse propagation that achieves these goals. It is based on the finite-difference time-domain (FDTD) method, which has been used extensively to model electromagnetic field propagation through media as diverse as human tissue and photonic structures.[29,30] The full-field simulation algorithms reported herein describe the electric polarization via equations of motion for a two-level system density matrix and utilize a correlation function treatment[7,31] of the relaxation. The formalism has the flexibility to incorporate real or complex multiterm energy gap (fluctuation) correlation functions, providing a means to include correlation functions from nonlinear spectroscopic measurements in the linear pulse propagation simulations. The algorithms are used to model the resonant propagation of ultrashort mid-IR pulses through optically-dense samples of HDO in liquid D_2O, showing the sensitivity of propagated fields to optical density, initial pulse chirp, and the correlation function itself. The next paper in this series will further explore propagation through HDO:D_2O by incorporating correlation functions from nonlinear infrared spectroscopy into the CF-FDTD simulations.[32] While the present formalism and simulations treat only linear propagation, they represent an important step toward modeling pulse propagation in nonlinear experiments, in which the ability to incorporate the non-Markovian response of the material is essential. Linear spectroscopy is, in theory, completely described in the frequency domain by the absorption coefficient and refractive index. However, the extension to nonlinear spectroscopy is accomplished more naturally in the time domain,[7] making the time-domain CF-FDTD method a more useful starting point for future modeling of nonlinear responses.

The organization of this paper is as follows: Section II provides a basic introduction to the FDTD method and reviews strategies for modeling electromagnetic field propagation in dispersive and dissipative media. This background material is followed by a description of the CF-FDTD formalism for real and complex material correlation functions in Sec. III. Section IV presents simulations that demonstrate the optical density and chirp dependence of linearly propagated ultrashort mid-IR pulse fields, focusing on resonant (with the OH-stretching vibration) propagation through samples of HDO in liquid D_2O. The simulation results are compared with experimentally-determined[20] electric fields. Simulations of fields propagated through media with different correlation functions for the OH-stretching vibration are also presented and discussed. Concluding remarks are given in Sec. V. Finally, the finite-differenced partial differential equations needed to simulate electric field propagation through materials described by real and complex correlation functions are provided in Appendices A and B, respectively.

II. BACKGROUND

The FDTD method is based on finite-differenced expressions for Maxwell's curl equations.[29,30] Derivatives in the curl equations are treated as second-order-accurate finite differences, and the resulting equations are advanced in time and space. The simulations presented in this article model the propagation of linearly-polarized electromagnetic fields in one dimension (along the z-axis) through a nonmagnetic, dielectric medium with no free charges. The curl equations are therefore

$$\frac{\partial H_y}{\partial t} = -\frac{1}{\mu_0}\frac{\partial E_x}{\partial z}, \tag{1}$$

$$\frac{\partial E_x}{\partial t} = -\frac{1}{\epsilon}\frac{\partial H_y}{\partial z} - \frac{1}{\epsilon}\frac{\partial P_x}{\partial t}, \tag{2}$$

where E_x, H_y, and P_x are the electric field, magnetic field, and electric polarization, respectively. The permeability, μ_0, is that of free space everywhere in the simulation, and the permittivity, ϵ, is that of the medium in which the fields are propagating, either free space or the (dielectric) solution.[33]

The focus of the present computational effort is the treatment of the polarization term in Eq. (2). In the general case, the polarization cannot be expressed as merely a constant times the electric field; therefore, it cannot be folded into the electric field derivative of Eq. (2) but must be treated explicitly. A number of FDTD strategies have been developed to treat media with a wavelength-dependent dielectric function. In the classical case, the recursive convolution FDTD method (Ref. 34) and its piecewise linear extension[35] have been successful in modeling Debye and Lorentz media. Taflove and co-workers have developed the auxiliary differential equation method for treating similar materials.[36] A variation on the RC-FDTD method that can simulate a classical underdamped or overdamped Brownian oscillator was recently employed by Beard and Schmuttenmaer to successfully model the propagation of femtosecond terahertz pulses through dielectric media, with and without optical perturbation.[14] While these algorithms are highly successful for their specific applications, they are purely classical; field interactions with high frequency vibrations are more properly modeled using a quantum mechanical treatment of the material, making a semi-classical approach desirable.

Joint Maxwell–Bloch and Maxwell–Schrödinger equations for two-level atoms have been incorporated into FDTD algorithms to perform semi-classical simulations. Tarasishin *et al.* developed a set of equations for the magnetic field, electric field, electric displacement, and population inversion of the system; their algorithm was used to test the McCall–Hahn area theorem and model light amplification.[37,38] Hughes modeled the breakdown of the area theorem[39] and

subfemtosecond x-ray generation[16] via carrier-wave Rabi flopping by performing FDTD simulations of high energy, ultrashort pulse propagation; the simulations solved the Bloch equations with a fourth-order RungewKutta method in tandem with the full-field Maxwell's equations. Ziolkowski and co-workers[40] have developed a FDTD algorithm that employs predictor–corrector integration and incorporates equations of motion for the density matrix of the system into the FDTD algorithm. This Maxwell–Bloch FDTD simulation technique has been used to simulate few-cycle pulse propagation[41] and model experimentally-observed carrier-wave Rabi flopping.[15] Ziolkowski's algorithm was only formulated in terms of the Bloch model for the relaxation of a system of two-level absorbers; however, its explicit treatment of all density matrix elements suggested the extension to the correlation function-based approach described herein.[42] The present paper demonstrates that Ziolkowski's approach can be modified to incorporate non-Markovian functions that describe the system dynamics in a more general fashion, thereby extending its range of applicability to dynamically more complex systems.

III. CF-FDTD FORMALISM

Two CF-FDTD algorithms are developed here. The first, and computationally more efficient, algorithm treats strictly real correlation functions; the resulting equations are identical to our corrected and extended version[42] of the Ziolkowski algorithm,[40] but have time-dependent coefficients that depend on integrals over the energy gap correlation function. The second algorithm uses a different representation of the vector of density matrix elements in Liouville space to incorporate complex correlation functions, resulting in a fully quantum-mechanical treatment of the medium.

A. Real correlation functions

1. Liouville equations of motion for a two-level system

The equations of motion for density matrix elements are developed naturally in the Liouville space representation of quantum mechanics.[7,31] The Liouville equation of motion is

$$\frac{\partial \hat{\rho}}{\partial t} = \frac{1}{\hbar}\hat{L}\hat{\rho}, \tag{3}$$

where $\hat{\rho}$ is a vector of density matrix elements and $\hat{L}$ is the Liouville operator, a matrix with elements given by the commutator of the Hamiltonian $[-i\hat{H},]$. The Hamiltonian for the present case can be written as the sum of an unperturbed part, $\hat{H}_0$, a term for the interaction with the electric field through the dipole operator, $\hat{H}_{\text{int}}$, and a term describing the relaxation of the system through interaction with the bath, $\hat{H}_{\text{relax}}$, yielding

$$\frac{\partial \hat{\rho}}{\partial t} = \frac{1}{\hbar}(\hat{L}_0 + \hat{L}_{\text{int}} + \hat{L}_{\text{relax}})\hat{\rho}. \tag{4}$$

The density matrix elements of the vector are then chosen such that all quantities in the calculations are real. To accomplish this, combinations of the elements of the 2×2 (Hilbert space representation) density matrix are formed,

$$\rho_1 = \rho_{ab} + \rho_{ba}, \tag{5}$$

$$\rho_2 = i(\rho_{ab} - \rho_{ba}), \tag{6}$$

$$\rho_3 = \rho_{bb} - \rho_{aa}, \tag{7}$$

where a and b refer to the ground and excited states, respectively, of the two-level system. Equations (5), (6), and (7) represent the in-phase (dispersive), out-of-phase (absorptive), and inversion components of the density matrix, respectively; conservation of probability $(\rho_{aa} + \rho_{bb} = 1)$ allows this simplification. The terms in Eq. (4) for the unperturbed and interaction parts of the Liouville equation are well known,[6,40] giving

$$\frac{\partial}{\partial t}\begin{pmatrix} \rho_1 \\ \rho_2 \\ \rho_3 \end{pmatrix} = \begin{pmatrix} 0 & \omega_0 & 0 \\ -\omega_0 & 0 & 2\frac{\mu}{\hbar}E_x \\ 0 & -2\frac{\mu}{\hbar}E_x & 0 \end{pmatrix}\begin{pmatrix} \rho_1 \\ \rho_2 \\ \rho_3 \end{pmatrix} + \hat{L}_{\text{relax}}\begin{pmatrix} \rho_1 \\ \rho_2 \\ \rho_3 - \rho_{30} \end{pmatrix}, \tag{8}$$

with transition dipole moment μ and resonant frequency ω_0. Here, E_x is the *complete* electric field calculated via the FDTD algorithm; the method therefore circumvents the RWA. This leaves only the relaxation term of the Liouville equation to be determined, and it is here that the correlation function treatment of the system–bath interaction is introduced.

2. Correlation function description of the relaxation

The correlation function formalism developed by Mukamel has found widespread use in the calculation of linear and nonlinear spectroscopic signals[7] and follows in the tradition of Gordon and Kubo's correlation function description of spectroscopy.[43,44] Within the second-order cumulant expansion and Condon approximations, Mukamel has shown that any linear or nonlinear signal can be expressed in terms of a two-time correlation function of the energy gap fluctuation between two molecular levels of interest,[7]

$$C(\tau_1) \equiv \frac{1}{\hbar^2}\langle U(\tau_1)U(0)\rho_a\rangle, \tag{9}$$

where U is the energy gap fluctuation and ρ_a is the ground state equilibrium density matrix of the bath. A key quantity appearing in the material response functions used to calculate spectroscopic signals is the line shape function $g(t)$, defined as

$$g(t) \equiv \int_0^t d\tau_2 \int_0^{\tau_2} d\tau_1 C(\tau_1). \tag{10}$$

The Fourier transform of $\exp[-g(t)]$ yields the line shape of the linear absorption spectrum.

By making an analogy between the relaxation superoperator treatment of relaxation[31] and the line shape function formalism,[7] the equations of motion for the density matrix can be expressed explicitly in terms of the first time derivative of the line shape function or, equivalently, an integral over $C(\tau_1)$. The derivation of the relaxation matrix follows the treatment of non-Markovian vibrational relaxation by Mukamel according to a partial time ordering prescription (POP) for the time evolution operator.[31] This time ordering is appropriate for condensed phase systems: the bath fluctuations have a Gaussian stationary distribution,[45] a reasonable choice for a liquid as the dynamics are the sum of many perturbations by the surroundings. The derivation of the relaxation matrix follows that given in Appendix A of Ref. 31 and is partially repeated here as Eqs. (11)–(23) to provide a more complete picture of the formalism development. First, the Liouville equation of Eq. (3) is rewritten as a matrix element,

$$\frac{\partial \rho_{ij}}{\partial t}=\frac{1}{\hbar}\sum_{kl} L_{ij,kl}\rho_{kl}, \tag{11}$$

where each element is still an operator in the bath space (the dipole perturbation is not present in the Liouville operator of Ref. 31 and so will not be included in this discussion). Note that the imaginary constant $-i$ is absorbed into the Liouville operator and the summation is over states a and b; redefinition of the density matrix elements as ρ_1, ρ_2, and ρ_3, will be performed after the equations of motion have been obtained. The relaxation of the density matrix elements is dictated by tetradic operators $\hat{G}$ and $\hat{F}$ for the dephasing (diagonal coupling) and population relaxation (off-diagonal coupling), respectively. As the population relaxation will always be treated as a single exponential decay, only the off-diagonal density matrix elements will be developed here. They are[31]

$$\frac{\partial \rho_{ab}}{\partial t}=-i\omega_0\rho_{ab}-i\hat{F}[\rho_{aa}-\rho_{bb}]-2i\hat{G}\rho_{ab}, \tag{12}$$

$$\frac{\partial \rho_{ba}}{\partial t}=i\omega_0\rho_{ba}-i\hat{F}[\rho_{bb}-\rho_{aa}]-2i\hat{G}\rho_{ba}, \tag{13}$$

with commutators (superoperators),

$$\hat{F}\equiv[F(|a\rangle\langle b|-|b\rangle\langle a|),], \tag{14}$$

$$\hat{G}\equiv[G_a|a\rangle\langle a|+G_b|b\rangle\langle b|,]. \tag{15}$$

The correlation function termed $\hat{W}$ in Ref. 31,

$$\hat{W}(t-\tau)=\langle \hat{L}_{\text{relax}}(t-\tau)\exp[\hat{L}_0(t-\tau)]\hat{L}_{\text{relax}}(0)\rangle, \tag{16}$$

is important for expressing the equations of motion in terms of the energy gap correlation function, which can be determined from the components of $\hat{W}$. For example,[31]

$$\begin{aligned}W_{ab,ab}(\tau)=&\sum_{\alpha,\beta} P(\alpha)\exp(-i\omega_{ab}\tau)\\&\times\{[L_{\text{relax}}(\tau)^{\beta\beta,\alpha\beta}_{ab,ab}L_{\text{relax}}(0)^{\alpha\beta,\alpha\alpha}_{ab,ab}\\&+L_{\text{relax}}(\tau)^{\beta\beta,\beta\alpha}_{ab,ab}L_{\text{relax}}(0)^{\beta\alpha,\alpha\alpha}_{ab,ab}\\&+L_{\text{relax}}(\tau)^{\alpha\alpha,\alpha\beta}_{ab,ab}L_{\text{relax}}(0)^{\alpha\beta,\alpha\alpha}_{ab,ab}\\&+L_{\text{relax}}(\tau)^{\alpha\alpha,\beta\alpha}_{ab,ab}L_{\text{relax}}(0)^{\beta\alpha,\alpha\alpha}_{ab,ab}]\\&+[L_{\text{relax}}(\tau)^{\alpha\alpha,\alpha\beta}_{ab,aa}L_{\text{relax}}(0)^{\alpha\beta,\alpha\alpha}_{aa,ab}]\\&+[L_{\text{relax}}(\tau)^{\alpha\alpha,\beta\alpha}_{ab,bb}L_{\text{relax}}(0)^{\beta\alpha,\alpha\alpha}_{bb,ab}]\},\end{aligned} \tag{17}$$

where α,β are bath states. In terms of functions F and $G_{a,b}$, Eq. (17) can be reduced to the following sum of correlation functions,[31]

$$\begin{aligned}W_{ab,ab}(\tau)=&2\exp(-i\omega_{ab}\tau)\{[\langle G_-(\tau)G_-(0)\rangle\\&+\langle G_-(-\tau)G_-(0)\rangle]\\&+[\langle G_-(\tau)G_+(0)\rangle+\langle G_-(-\tau)G_+(0)\rangle]\}\\&+[\langle F(\tau)F(0)\rangle+\langle F(-\tau)F(0)\rangle],\end{aligned} \tag{18}$$

where

$$G_+\equiv\tfrac{1}{2}(G_a+G_b),\quad G_-\equiv\tfrac{1}{2}(G_a-G_b) \tag{19}$$

represent the average transition energy and gap fluctuations, respectively. $W_{ba,ba}(\tau)$ is the only other nonzero off-diagonal component for this system (i.e., where at least one of the subscripts is ab or ba), as F and G are assumed to be uncorrelated and the contribution of the correlation function for F to the off-diagonal dephasing terms is ignored.[31]

Using the POP and truncating the time integrals to second order in the cumulant expansion approximation, the equation of motion for the system density matrix becomes[31]

$$\frac{\partial \hat{\rho}}{\partial t}=\hat{L}_0\hat{\rho}-\left(\int_0^t d\tau\hat{\Omega}(t-\tau)\right)\hat{\rho}, \tag{20}$$

where

$$\hat{\Omega}(t-\tau)=\hat{W}(t-\tau)\exp[-\hat{L}_0(t-\tau)]. \tag{21}$$

For the formalism of this article, the integral in Eq. (20) is the relaxation Liouville operator, $\hat{L}_{\text{relax}}$, of Eq. (4). The incorporation of the line shape function into the formalism is demonstrated by considering one of the off-diagonal density matrix elements,[31]

$$\frac{\partial \rho_{ba}}{\partial t}=-i\omega_{ba}\rho_{ba}-\left(\int_0^t d\tau A(\tau)\right)\rho_{ba}, \tag{22}$$

where

$$\begin{aligned}A(\tau)=&2\{[\langle G_-(\tau)G_-(0)\rangle+\langle G_-(-\tau)G_-(0)\rangle]\\&+[\langle G_-(\tau)G_+(0)\rangle+\langle G_-(-\tau)G_+(0)\rangle]\}\\&+e^{i\omega_{ba}\tau}[\langle F(\tau)F(0)\rangle+\langle F(-\tau)F(0)\rangle].\end{aligned} \tag{23}$$

The connection of this equation with the line shape function formalism can be understood by examining the quantities $G_\pm(\tau)$ and $F(\tau)$. $G_-(\tau)$ and $G_+(\tau)$ represent the energy gap fluctuation and fluctuation in average energy, respectively, while $F(\tau)$ represents population fluctuations.[31] The correlation function $A(\tau)$ describes the overall dephasing of this density matrix element. If population relaxation contributes only negligibly to dephasing (often the case at room

temperature) and fluctuations in the energy gap are not correlated with fluctuations in the average energy, then the correlation function in Eq. (23) contains only autocorrelations of $G_-(\tau)$. Therefore, $A(\tau)$ measures energy gap fluctuation correlations. By analogy with the correlation function formalism presented in Ref. 7, $A(\tau)$ therefore plays the role of the correlation function, $C(\tau)$ [Eq. (9)]. Further comparison to the formula for the line shape function in Eq. (10) reveals that Eq. (22) can be recast in terms of the time derivative of $g(t)$,

$$\frac{\partial \rho_{ba}}{\partial t} = -i\omega_{ba}\rho_{ba} - \dot{g}(t)\rho_{ba}. \tag{24}$$

A similar equation can be written for the other off-diagonal element ρ_{ab}. $\hat{L}_{\text{relax}}$ can then be formed via the combinations of elements prescribed by Eqs. (5) and (6). For a real $g(t)$ (the complex case will be treated in the next section), the relaxation matrix becomes simply

$$L_{\text{relax}} = \begin{pmatrix} -\dot{g}(t) & 0 & 0 \\ 0 & -\dot{g}(t) & 0 \\ 0 & 0 & -\dfrac{1}{T_1} \end{pmatrix}, \tag{25}$$

where, as stated above, correlations between the diagonal and off-diagonal elements of the tetradic relaxation superoperator have been neglected.[31] Combining Eqs. (8) and (25) gives the equation of motion for the density matrix,

$$\frac{\partial}{\partial t}\begin{pmatrix} \rho_1 \\ \rho_2 \\ \rho_3 \end{pmatrix} = \begin{pmatrix} 0 & \omega_0 & 0 \\ -\omega_0 & 0 & 2\dfrac{\mu}{\hbar}E_x \\ 0 & -2\dfrac{\mu}{\hbar}E_x & 0 \end{pmatrix}\begin{pmatrix} \rho_1 \\ \rho_2 \\ \rho_3 \end{pmatrix} + \begin{pmatrix} -\dot{g}(t) & 0 & 0 \\ 0 & -\dot{g}(t) & 0 \\ 0 & 0 & -\dfrac{1}{T_1} \end{pmatrix}\begin{pmatrix} \rho_1 \\ \rho_2 \\ \rho_3 - \rho_{30} \end{pmatrix}, \tag{26}$$

where the initial inversion ρ_{30} has been subtracted from ρ_3 in the relaxation term. The population relaxation is treated as a single exponential with lifetime T_1 in all cases.

The polarization of the medium is linked to the density matrix through the relation

$$P_x(t) = -N\mu[\rho_{ab}(t) + \rho_{ba}(t)] = -N\mu\rho_1(t), \tag{27}$$

with N equal to the number density of two-level absorbers. Therefore, the coupled Maxwell–Liouville equations for the fields and density matrix elements are

$$\frac{\partial H_y}{\partial t} = -\frac{1}{\mu_0}\frac{\partial E_x}{\partial z}, \tag{28}$$

$$\frac{\partial E_x}{\partial t} = -\frac{1}{\epsilon}\frac{\partial H_y}{\partial z} - \frac{1}{\epsilon}\frac{\partial P_x}{\partial t} = -\frac{\partial H_y}{\partial z} - \frac{N\mu}{\epsilon}\dot{g}(t)\rho_1 + \frac{N\mu\omega_0}{\epsilon}\rho_2, \tag{29}$$

$$\frac{\partial \rho_1}{\partial t} = \omega_0\rho_2 - \dot{g}(t)\rho_1, \tag{30}$$

$$\frac{\partial \rho_2}{\partial t} = -\omega_0\rho_1 + 2\frac{\mu}{\hbar}E_x\rho_3 - \dot{g}(t)\rho_2, \tag{31}$$

$$\frac{\partial \rho_3}{\partial t} = -2\frac{\mu}{\hbar}E_x\rho_2 - \frac{1}{T_1}(\rho_3 - \rho_{30}). \tag{32}$$

Equations (29)–(32) are finite-differenced after multiplying the density matrix elements by $\exp[-g(t)]$ for ρ_1 and ρ_2 and $\exp(-t/T_1)$ for ρ_3. These correlation function-based FDTD (CF-FDTD) equations are given in Appendix A, along with additional details about the algorithm. The resulting equations show that knowledge of $g(t)$ and its first time derivative [or, equivalently, $C(\tau)$ and its integrals] is sufficient to determine the coherence relaxation terms in the density matrix equation of motion. The time derivative is a linear operator; therefore, any sum of line shape functions representing, for example, multiple Brownian oscillators can be incorporated into the algorithm.

B. Complex correlation functions

The description of the system–bath interaction with a real line shape function is applicable when a stochastic or otherwise classical view of the relaxation is taken, as is often the case in practice. However, this approach does not necessarily capture a fully microscopic (i.e., quantum-mechanical) picture of molecular interactions. The neglect of an imaginary part of the line shape function inherent to a stochastic description results in a model that does not satisfy the fluctuation-dissipation theorem, i.e., the bath influences the system, but not vice versa.[7] When applied to vibrational spectroscopy, this assumes that low-frequency vibrations coupled to the mode of interest do not themselves undergo modulation of their frequencies; this may not be a valid assumption for strongly-interacting systems. Furthermore, without an imaginary component of the line shape function, a frequency or Stokes-shift of the transition is not possible. For a more general treatment of molecular relaxation, particularly for future extensions to nonlinear responses, the CF-FDTD algorithm should be expanded to incorporate complex line shape functions.

The equations for simulating pulse propagation through media with a complex line shape function are analogous to the real line shape case. However, the need to include the complex conjugate of $g(t)$ ($g^*(t) \neq g(t)$) precludes the use of the same vector of density matrix elements as in Eqs. (5)–(7). A convenient means of representing the vector is to not combine the off-diagonal density matrix elements, but leave them as the first two elements of the vector. Hence, the vector elements are

$$\rho_1 = \rho_{ab}, \tag{33}$$

$$\rho_2 = \rho_{ba}, \tag{34}$$

$$\rho_3 = \rho_{bb} - \rho_{aa}, \tag{35}$$

where ρ_3 is still the inversion. Following the same procedure as in Sec. III A, the Liouville equation of motion becomes

$$\frac{\partial}{\partial t}\begin{pmatrix}\rho_1\\ \rho_2\\ \rho_3\end{pmatrix} = i\begin{pmatrix}\omega_0 & 0 & -\frac{\mu}{\hbar}E_x\\ 0 & -\omega_0 & \frac{\mu}{\hbar}E_x\\ -2\frac{\mu}{\hbar}E_x & 2\frac{\mu}{\hbar}E_x & 0\end{pmatrix}\begin{pmatrix}\rho_1\\ \rho_2\\ \rho_3\end{pmatrix} + \begin{pmatrix}-\dot{g}(t) & 0 & 0\\ 0 & -\dot{g}^*(t) & 0\\ 0 & 0 & -\frac{1}{T_1}\end{pmatrix}\begin{pmatrix}\rho_1\\ \rho_2\\ \rho_3-\rho_{30}\end{pmatrix}. \tag{36}$$

The polarization now is expressed as a sum of vector elements,

$$P_x(t) = -N\mu[\rho_1(t) + \rho_2(t)], \tag{37}$$

giving the following Maxwell–Liouville equations:

$$\frac{\partial E_x}{\partial t} = -\frac{\partial H_y}{\partial z} - \frac{N\mu}{\epsilon}\{[i\omega_0 - \dot{g}(t)]\rho_1 - [i\omega_0 + \dot{g}^*(t)]\rho_2\}, \tag{38}$$

$$\frac{\partial \rho_1}{\partial t} = [i\omega_0 - \dot{g}(t)]\rho_1 - i\frac{\mu}{\hbar}E_x\rho_3, \tag{39}$$

$$\frac{\partial \rho_2}{\partial t} = -[i\omega_0 + \dot{g}^*(t)]\rho_2 + i\frac{\mu}{\hbar}E_x\rho_3, \tag{40}$$

$$\frac{\partial \rho_3}{\partial t} = 2i\frac{\mu}{\hbar}E_x(\rho_2 - \rho_1) - \frac{1}{T_1}(\rho_3 - \rho_{30}). \tag{41}$$

where the equation for the magnetic field is the same as Eq. (28). Note that $(\partial\rho_1/\partial t)^* = \partial\rho_2/\partial t$, as expected. It can be shown that these equations are equivalent to Eqs. (29)–(32) when $g(t) = g^*(t)$ and the coherence elements of the density matrix are redefined according to Eqs. (5) and (6). The finite-differenced equations and time-dependent coefficients for simulations using this material description are supplied in Appendix B.

IV. SIMULATION RESULTS AND DISCUSSION

To demonstrate the utility and versatility of this computational approach, the CF-FDTD algorithms are used to simulate the resonant propagation of ultrashort mid-IR pulses through samples of isotopically-diluted water (HDO in D_2O). Recent experimental measurements of pulse propagation through this system using the cross-correlation frequency-resolved optical gating (XFROG) (Ref. 46) technique have determined the electric field profiles before and after traversing optically dense solutions.[20] The measurements, which allowed extraction of the pulse field amplitude and phase via the XFROG analysis, examined the effects of optical density and initial pulse chirp on the field profiles resulting from propagation through a concentration series of samples. As a number of recent nonlinear mid-IR spectroscopic measurements have proposed correlation functions for the OH-stretching vibration,[27,47–49] this system also provides a unique opportunity to simulate experimental pulse propagation results using parameters obtained almost exclusively from the literature. Furthermore, comparison between experiment and simulation allows examination of how well the proposed functions describe early-time relaxation. The exquisite sensitivity of the FID beats to early time dipolar relaxation results in beat patterns that depend on the details of the line shape function in the first ~200 fs: even if line shape functions yield very similar absorption band shapes, the field modulation due to interaction with high OD samples can distinguish them if the spectra resulting from these functions do not completely overlap. This phenomenon will be explored in depth in the next paper in this series.[32] The purpose of the simulations presented herein is to illustrate the concentration, chirp, and correlation function dependence of the propagated fields as a demonstration of the general capabilities of the CF-FDTD algorithms.

The experimental details were reported in Ref. 20. The number density of OH oscillators, N, was determined from the concentration of the HDO:D_2O samples to be $\sim 1.7–6.7\times 10^{26}$ m^{-3}. The transition dipole moment, μ, was calculated from the integrated absorption coefficient[50] via the Einstein B coefficient; the value of μ was 7.612×10^{-31} C m. The permittivity of the solution was set to that of neat D_2O at 3400 cm^{-1} ($\epsilon = 1.457\times 10^{-11}$ J^{-1} C^2 m^{-1}),[51] which is close to the OH-stretching absorption maximum. In addition, the initial inversion was -1 for all simulations; that is, all molecules were initially in the ground vibrational state. The electric field amplitude and phase parameters of the driving pulses were obtained from XFROG measurements of the instrument response and pulse after propagation through the D_2O solvent.[20] The initial pulses had a Gaussian envelope and carrier frequency matched to that of the mid-IR pulse, which was resonant with the OH-stretching transition. The initial pulse field duration was set to 88 fs, which assumed propagation through neat D_2O and the CaF_2 windows prior to the PC-FDTD calculation. The group velocity dispersion (GVD) was determined from polynomial fits to the temporal phase determined by the XFROG algorithm. The form of the electric field of the initial pulse was therefore

$$E_x(t) = E_0 \exp\left[-2\ln(2)\left(\frac{t}{\tau}\right)^2\right]\sin[\omega_p t + a t^2], \tag{42}$$

where E_0 is the initial magnitude (arbitrarily set to 1.0 for all calculations; variation of E_0 by several orders of magnitude in either direction did not affect the results), τ is the pulse duration, ω_p is the pulse carrier frequency, and a is the GVD. Addition of third order dispersion (TOD), determined by the same polynomial fits to the XFROG data, did not significantly change the resulting profiles; therefore, TOD was not included in the simulations reported herein.

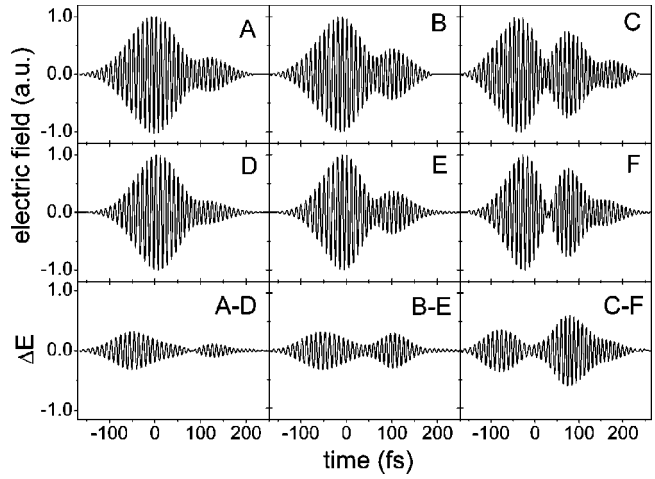

FIG. 1. Dependence of simulated and experimental field profiles on OH concentration. First row: experiment; second row: simulation; third row: ΔE =experiment − simulation. (A, D) 1:200; (B, E) 1:100; and (C, F) 1:50 HDO:D_2O mole ratios. Simulated and experimental fields are normalized to a maximum of one.

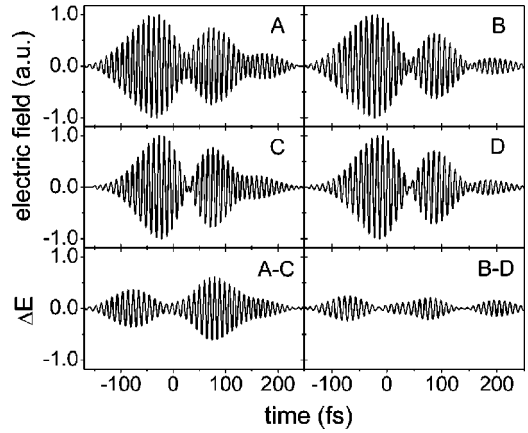

FIG. 2. Dependence of simulated and experimental fields on driving pulse chirp; 1:50 HDO:D_2O sample. First row: experiment; second row: simulation; third row: ΔE=experiment − simulation. GVD=(A, C) 2×10^{-5} fs^{-2}; (B, D) 7×10^{-6} fs^{-2}. Simulated and experimental fields are normalized to a maximum of one.

A. Optical density and chirp dependence

Experimental and simulated electric fields propagated through 200 μm path length samples of 1:200, 1:100, and 1:50 HDO:D_2O solutions. Figure 1 shows the field profiles from the experimental data and simulations using a simple Bloch model for the relaxation; the dephasing time was 43 fs, selected to match the full width at half maximum (FWHM) spectral width of the absorption band, and the population relaxation time of 700 fs was obtained from the literature.[49] The experimental and simulated fields are shown in the first and second rows of Fig. 1, respectively, and the difference (experiment-simulation) is displayed in the third row. The number density of OH oscillators in the sample increases from left to right. Variation of T_1 by ± 50 fs did not significantly alter the simulated fields, consistent with the linear response and fixed total dephasing time. The simulated fields show the same trend as that observed in experiment: the FID beat grows in magnitude with increasing concentration, with a second FID beat being generated in the most optically-dense sample. A phase shift occurs between the lobes of the field profiles, as would be expected from the phase relationships between the driving pulse, polarization, and FID.[22] However, the shift is not prompt and is obscured in the nodal regions, presumably due to the residual chirp ($\sim 2\times10^{-5}$ fs^{-2}) on the pulses; this was observed in the XFROG results as temporal phase jumps with finite slopes.[20]

To further investigate the influence of pulse chirp on the simulated profiles, comparisons were made between fields propagated through the 1:50 HDO:D_2O solution with different chirps, using GVD parameters derived from the corresponding experimentally-measured input pulses.[20] In the experiments, the chirp was varied for the 1:50 HDO:D_2O solution by changing the amount of dispersion compensation before the sample cell. Figure 2 demonstrates the effect of the initial pulse chirp on the propagated fields. The GVD in Figs. 2(A) and 2(C) was $\sim 2\times10^{-5}$ fs^{-2} and that for Figs. 2(B) and 2(D) was $\sim 7\times10^{-6}$ fs^{-2}. It is clear that the destructive interference between the driving pulse and FID(s) is more complete when the pulse is closer to the transform limit, as was observed in the amplitude and phase profiles obtained from experiment.[20] The CF-FDTD simulations successfully reproduce this trend.

The simulated fields shown in Figs. 1 and 2 arise from interaction with a homogeneously-broadened Bloch medium. Qualitatively, the agreement between experiment and simulation is quite good; note that no parameters were adjusted for the simulations. However, it is evident that the simulation does not quantitatively account for the observed fields, as is especially apparent for the more chirped pulses. The next issue to consider for its influence on FID beat patterns is the form of the correlation function, as the Bloch model does not provide a realistic description of vibrational relaxation in water. The energy gap correlation function for the OH-stretching vibration of water has been pursued intensely since the development of short-pulse mid-IR sources in the 3000 nm spectral region. Despite remaining disagreements about the details of the relaxation, the body of evidence amassed to date indicates, not surprisingly, that the relaxation is non-Markovian in character.[27,47–49,52,53] The availability of several correlation functions affords the unique opportunity to examine how they are manifested in the propagation of mid-IR pulses through these samples via the CF-FDTD algorithm; this investigation will be detailed in the second paper in this series.[32] In the next section, a series of basic correlation function types are used to demonstrate the flexibility of the CF-FDTD algorithms in treating a variety of line shape functions with different degrees of memory.

B. Correlation function dependence

One obvious drawback of the Bloch model is its inability to capture more than one kind of relaxation. There is only one adjustable parameter, the dephasing time T_2, to describe the coherence dynamics. Figures 3(A)–3(C) show that the effect of changing this parameter is a simple increase of the FID beat magnitude as T_2 is varied from 38 to 48 fs, with some modification of the relative magnitudes of the beats. A

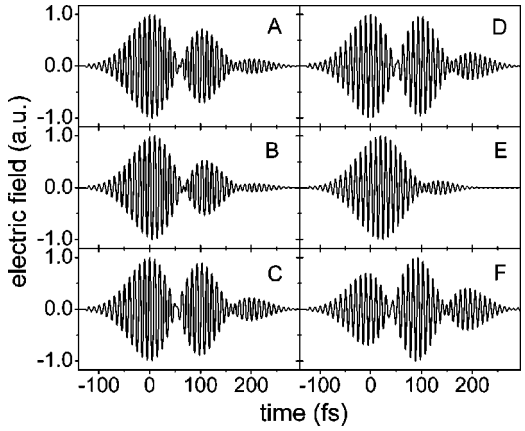

FIG. 3. Comparison of propagation through a Bloch medium and a medium described by a single Kubo function; 1:50 HDO:D_2O sample. (A–C) are Bloch media, and (D–F) are Kubo media sharing the same 1/e decay time. (A) $T_2=43$ fs; (B) $T_2=38$ fs; (C) $T_2=48$ fs; (D) $\Lambda^{-1}=\Delta^{-1}=43$ fs ($\kappa=1$); (E) $\Lambda^{-1}=99$ fs; $\Delta^{-1}=49$ fs ($\kappa=0.5$); (F) $\Lambda^{-1}=16$ fs; $\Delta^{-1}=32$ fs ($\kappa=2.0$). All fields are normalized to a maximum of one.

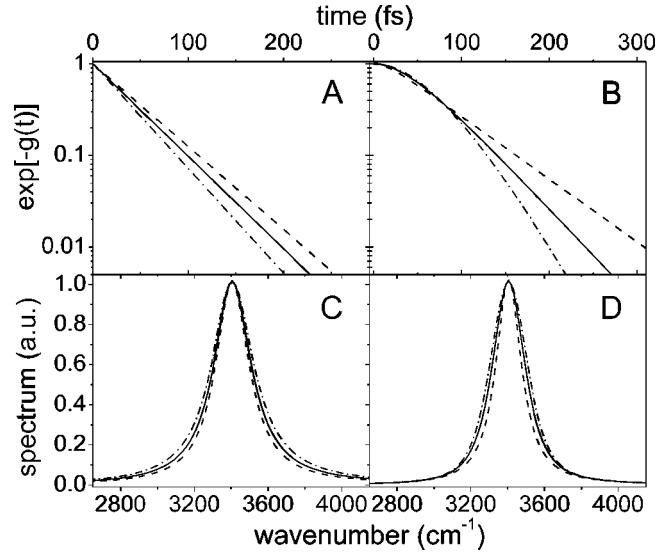

FIG. 4. Response functions $\exp[-g(t)]$ (A,B) and power spectra (C,D) corresponding to the media of Fig. 3. Panels (A) and (C) are characteristics of the Bloch media, with solid: $T_2=43$ fs; dotted–dashed: $T_2=38$ fs; dashed: $T_2=48$ fs. Panels (B) and (D) represent the Kubo medium, with solid: $\kappa=1.0$; dotted–dashed: $\kappa=0.5$; dashed: $\kappa=2.0$.

more flexible model employs the Kubo function, an exponential correlation function which interpolates between Markovian (Bloch-type) and inhomogeneous (Gaussian) behavior by the relative magnitudes of its correlation time, Λ^{-1}, and root mean square fluctuation strength, Δ

$$C(\tau_1)=\Delta^2 \exp[-\Lambda\tau_1]. \tag{43}$$

A commonly-used measure of the homogeneous versus inhomogeneous character is the dimensionless parameter κ, defined as[7]

$$\kappa \equiv \frac{\Lambda}{\Delta}. \tag{44}$$

Inhomogeneous behavior is obtained for $\kappa \ll 1$, when the fluctuation magnitude is much larger than its time scale. Homogeneous behavior occurs in the opposite limit of $\kappa \gg 1$.

Keeping the same $1/e$ time for the response function decay, the shape of the Kubo response function can be readily altered. A simulation using a single Kubo function with $\Lambda^{-1}=\Delta^{-1}=43$ fs ($\kappa=1$) is shown in Fig. 3(D). The electric field profiles of Figs. 3(E) and 3(F) are obtained by changing κ to 0.5 and 2.0, respectively, but keeping the same 1/e time of the response function. The corresponding response functions and power spectra for the Bloch and Kubo media are provided in Fig. 4. The power spectra for each set of responses are similar, but the relative weight given to the spectral wings changes with κ for the Kubo functions. The more homogeneous Kubo response that gives rise to the field in Fig. 3(F) decays more slowly than the intermediate case, leading to enhanced beats. Conversely, the more Gaussian-type response decays more quickly following a slower initial decay and rapidly damps out the FID beats. As can be observed in Figs. 3 and 4, the electric field profiles after propagation are particularly sensitive to these details of the coherence relaxation; the time-domain propagated fields enhance the distinction among the responses. This characteristic will become important when considering non-Markovian functions obtained from third-order nonlinear spectroscopic measurements.[32]

V. CONCLUSIONS

The CF-FDTD algorithms detailed in this paper constitute a successful merging of the full-field FDTD method with the correlation function picture of spectroscopy widely used to describe ultrafast spectroscopic signals. Through explicit treatment of the density matrix elements of a two-level system, these algorithms permit the simulation of pulse interactions with media that relax on multiple time scales. The experimentally-observed FID beat features from pulse propagation through water are successfully reproduced using this method; the case of OH-stretching vibrational dynamics in water illustrates the power of this approach and the sensitivity of the fields to the fastest dynamics. Furthermore, the ability to incorporate correlation functions from nonlinear optical spectroscopy into the CF-FDTD algorithm allows a comparison of experimental pulse propagation results with simulation, as will be demonstrated in the next paper in this series.[32] This is a potentially useful means to assess the suitability of the early-time medium response described by a given correlation function. The CF-FDTD method presented in this paper is sufficiently general to model dipolar molecular responses in media with complicated, multi-time dynamics. The incorporation of the two-time energy gap fluctuation correlation function into the CF-FDTD approach allows unprecedented flexibility in describing material response functions in a full-field calculation; non-Markovian relaxation can be treated naturally in this representation.

In addition to the description of the OH-stretching mode relaxation, a number of issues remain to be addressed in order to more accurately reproduce the experimentally-determined pulse fields after linear propagation. The algo-

rithms reported herein focus on the response of the two-level absorbers in resonance with the incoming pulse. However, the solvent (in this case D_2O) can also influence the resulting field profiles through nonresonant material dispersion effects. This was apparent in pulse propagation measurements, which showed significant broadening of the pulse (increase in duration of ~10 fs) after traveling through the neat D_2O solvent compared to the empty sample cell. In the present simulations, this effect is treated in a simplistic manner, setting the permittivity to that of D_2O and "prebroadening" the pulses to what they would be after propagation through the solvent alone. It can be observed in the field differences (bottom rows of Figs. 1 and 2) that the breadth of the driving pulse after propagation is consistently underestimated with respect to the experiment, which may result from the neglect of the solvent dispersion during propagation. Furthermore, changing the dielectric constant in the two-level medium to the permittivity of free space increases the relative magnitude of the FID beats with respect to the main pulse (not shown). Inclusion of dynamic dispersive broadening by, for example, interleaving a recursive-convolution FDTD algorithm[34] with the CF-FDTD algorithm would lead to a more accurate picture of the pulse propagation that may account for some of the driving pulse broadening missing from the simulated fields, as well as some mismatch in FID beat magnitudes. Uncertainty in experimental parameters could also contribute to discrepancies between experimental and simulated fields. However, variation of the path length by ±10% did not improve the agreement of simulated fields with experiment. Similarly, changing the number density by ±10% resulted in worse agreement with experiment, suggesting that uncertainty in concentration is not responsible for these discrepancies.

The main purpose of the development of the CF-FDTD method is to simulate the effects of pulse propagation on *nonlinear* spectroscopic measurements; the linear propagation algorithms presented in this article represent an important first step toward this goal. The modeling of nonlinear field–matter interactions could proceed in a number of ways. In the most simplistic case, this could be accomplished with the present linear algorithm by assuming that the nonlinear signal (calculated by other means) is generated at the beginning of the sample cell and propagating the signal linearly through the remainder of the material. More rigorous treatment will require incorporation of the nonlinear response into the algorithm, as has been accomplished in pump–probe pulse envelope simulations using the Maxwell–Bloch equations for both the linear and third-order nonlinear polarizations.[17] Third order nonlinearities have been modeled in FDTD algorithms by Taflove[54] and Ziolkowski,[55] who incorporated both Kerr and Raman nonlinearities into phenomenological material responses. A similar treatment, modified for a quantum-mechanical material, could be used to extend the algorithms presented here. In the case of water, the nearby $v=1$ to $v=2$ transition also must be taken into account for third-order responses;[27,47–49,52,53,56–58] a two-level system approach is therefore insufficient to properly model these nonlinear spectroscopic measurements. However, the density matrix-based approach is amenable to an extension to three-level systems, and such an algorithm for Bloch relaxation has recently been reported.[59] Therefore, the CF-FDTD method has the potential to successfully calculate the effects of propagation on nonlinear mid-IR spectroscopic signals from multi-level systems with multi-time, non-Markovian relaxation.

ACKNOWLEDGMENTS

The author is indebted to Professor Norbert F. Scherer (University of Chicago) for guidance during this work and valuable contributions to the manuscript. The author thanks Professor Richard Ziolkowski (University of Arizona) for conversations regarding his original paper on the predictor–corrector FDTD method. This work was supported financially by the Consortium for Nanoscience Research and the Institute for Biophysical Dynamics Seed Fund. The author also thanks the National Science Foundation for a Graduate Research Fellowship (1998-2001) and the University of Chicago for a William Rainey Harper Dissertation Fellowship.

APPENDIX A: FINITE-DIFFERENCE EQUATIONS FOR REAL CORRELATION FUNCTIONS

Equations (28)–(32) for the fields and density matrix elements form the basis for the CF-FDTD algorithm. Before finite-differencing, the density matrix elements are recast in a reduced form for computational simplicity, as outlined by Ziolkowski *et al.* The three reduced quantities are defined as[40]

$$\rho_1(z,t)=u_1(z,t)e^{-g(t)}, \tag{A1}$$

$$\rho_2(z,t)=u_2(z,t)e^{-g(t)}, \tag{A2}$$

$$\rho_3(z,t)=\rho_{30}+u_3(z,t)e^{-(t/T_1)}. \tag{A3}$$

The Maxwell–Liouville equations for the electric field and reduced density matrix elements then become

$$\frac{\partial E_x}{\partial t}=-\frac{1}{\epsilon}\frac{\partial H_y}{\partial z}-A(t)u_1+B(t)u_2, \tag{A4}$$

$$\frac{\partial u_1}{\partial t}=\omega_0 u_2, \tag{A5}$$

$$\frac{\partial u_2}{\partial t}=-\omega_0 u_1+C_+(t)E_x u_3+D(t)E_x, \tag{A6}$$

$$\frac{\partial u_3}{\partial t}=-C_-(t)E_x u_2. \tag{A7}$$

The time-dependent coefficients in Eqs. (A4)–(A7) are

$$A(t)=\frac{N\mu}{\epsilon}\dot{g}(t)e^{-g(t)}, \tag{A8}$$

$$B(t)=\frac{N\mu\omega_0}{\epsilon}e^{-g(t)}, \tag{A9}$$

$$C_\pm(t)=2\frac{\mu}{\hbar}e^{\pm g(t)}e^{\mp(t/T_1)}, \tag{A10}$$

$$D(t)=2\frac{\mu}{\hbar}\rho_{30}e^{g(t)}. \tag{A11}$$

The equations are finite-differenced according to the standard prescription (second-order accurate),[29,30] with the magnetic field shifted one half space (Δz) and time (Δt) step from the electric field and density matrix equations. For finite-differencing, terms on the right hand sides of Eqs. (A4)–(A7) that contain u_i treat each u_i as the average of its value for the current and previous time locations. The space and time locations of the field and density matrix elements are set according to the Yee cell representation,[60] with the density matrix elements located at the same positions as the electric field. With the time-dependent coefficients defined as in Eqs. (A8)–(A11), the resulting finite-differenced equations are the same as the corrected[42] versions of those in the appendix of Ziolkowski's original paper [Eqs. (A4a)–(A4e)]:[40]

$$H_y\left(m+\frac{1}{2},n+\frac{1}{2}\right)=H_y\left(m+\frac{1}{2},n-\frac{1}{2}\right)-\frac{\Delta t}{\mu_0\Delta z}\times[E_x(m+1,n)-E_x(m,n)], \tag{A12}$$

$$E_x(m,n+1)=E_x(m,n)-\frac{\Delta t}{\epsilon\Delta z}\left[H_y\left(m+\frac{1}{2},n+\frac{1}{2}\right)-H_y\left(m-\frac{1}{2},n+\frac{1}{2}\right)\right]-\Delta tA\left(n+\frac{1}{2}\right)\frac{1}{2}\times[u_1(m,n+1)+u_1(m,n)]+\Delta tB\times(n+\tfrac{1}{2})\,\tfrac{1}{2}[u_2(m,n+1)+u_2(m,n)], \tag{A13}$$

$$u_1(m,n+1)=u_1(m,n)+\Delta t\omega_0\,\tfrac{1}{2}[u_2(m,n+1)+u_2(m,n)], \tag{A14}$$

$$u_2(m,n+1)=u_2(m,n)-\Delta t\omega_0\,\tfrac{1}{2}[u_1(m,n+1)+u_1(m,n)]+\Delta t\,\tfrac{1}{2}[E_x(m+1,n)-E_x(m,n)]\{C_+(n+\tfrac{1}{2})\,\tfrac{1}{2}[u_3(m,n+1)+u_3(m,n)]+D(n+\tfrac{1}{2})\}, \tag{A15}$$

$$u_3(m,n+1)=u_3(m,n)-\Delta tC_-(n+\tfrac{1}{2})\{\tfrac{1}{2}[E_x(m+1,n)-E_x(m,n)]\times\tfrac{1}{2}[u_2(m,n+1)+u_2(m,n)]\}, \tag{A16}$$

where m and n are the indices of the space and time step locations, respectively. The equation for H_y is advanced in the standard "leapfrog" fashion, while the remaining equations for E_x and u_1-u_3 are evaluated with a predictor–corrector algorithm.[40]

The platform chosen for the computations was MATLAB 6.5, which served as a natural environment due to its vectorizing capabilities. The routine contained on the order of 100 lines of executable code, depending on the response function chosen by the user. Evaluation of ~18 000 space steps and ~39 000 time steps took approximately 1–1.5 h to run on a desktop PC with a 533 MHz system bus, 2.4 GHz processor, and 512 MB RAM running Windows XP; the sample was spatially discretized at λ/100 and had a time step at half the Courant stability criterion.[29,30] Discretization at the λ/200 level resulted in calculated fields essentially identical with those at the λ/100 level. The code was tested by the successful observation of the self-induced transparency of a $2\pi\,\mathrm{sech}^2$ pulse in a Bloch medium.

APPENDIX B: FINITE-DIFFERENCE EQUATIONS FOR COMPLEX CORRELATION FUNCTIONS

The FDTD expression of Eqs. (38)–(41) for the complex response function follows that for the real response function as developed in Appendix A. The reduced forms of the new density matrix (vector) elements are identical to Eqs. (A1)–(A3), except that the complex conjugate $g^*(t)$ appears in the expression for ρ_2,

$$\rho_2(z,t)=u_2(z,t)e^{-g^*(t)}. \tag{B1}$$

The reduced equations are

$$\frac{\partial E_x}{\partial t}=-\frac{1}{\epsilon}\frac{\partial H_y}{\partial z}+A(t)u_1-B(t)u_2, \tag{B2}$$

$$\frac{\partial u_1}{\partial t}=i\omega_0u_1+C_+(t)E_xu_3+D(t)E_x, \tag{B3}$$

$$\frac{\partial u_2}{\partial t}=-i\omega_0u_2+C_+^*(t)E_xu_3+D^*(t)E_x, \tag{B4}$$

$$\frac{\partial u_3}{\partial t}=C_-(t)E_xu_1+C_-^*(t)E_xu_2, \tag{B5}$$

with time-dependent coefficients,

$$A(t)=\frac{N\mu}{\epsilon}[i\omega_0-\dot{g}(t)]e^{-g(t)}, \tag{B6}$$

$$B(t)=\frac{N\mu}{\epsilon}[i\omega_0+\dot{g}^*(t)]e^{-g^*(t)}, \tag{B7}$$

$$C_+(t)=-i\frac{\mu}{\hbar}e^{g(t)}e^{-(t/T_1)}, \tag{B8}$$

$$C_-(t)=-2i\frac{\mu}{\hbar}e^{-g(t)}e^{(t/T_1)}, \tag{B9}$$

$$D(t)=-i\frac{\mu}{\hbar}\rho_{30}e^{g(t)}. \tag{B10}$$

Using the same strategy as for the real correlation function case, the finite-differenced equations for the more general complex function case are

$$E_x(m,n+1)=E_x(m,n)-\frac{\Delta t}{\epsilon\Delta z}\left[H_y\left(m+\frac{1}{2},n+\frac{1}{2}\right)-H_y\left(m-\frac{1}{2},n+\frac{1}{2}\right)\right]+\Delta tA\left(n+\frac{1}{2}\right)\frac{1}{2}\times[u_1(m,n+1)+u_1(m,n)]$$

$$-\Delta t B(n+\tfrac{1}{2})\,\tfrac{1}{2}[u_2(m,n+1) + u_2(m,n)], \tag{B11}$$

$$u_1(m,n+1) = u_1(m,n) + i\Delta t\omega_0\,\tfrac{1}{2}[u_1(m,n+1) + u_1(m,n)] + \Delta t\,\tfrac{1}{2}[E_x(m+1,n) - E_x(m,n)]\{C_+(n+\tfrac{1}{2})\,\tfrac{1}{2}[u_3(m,n+1) + u_3(m,n)] + D(n+\tfrac{1}{2})\}, \tag{B12}$$

$$u_2(m,n+1) = u_2(m,n) - i\Delta t\omega_0\,\tfrac{1}{2}[u_2(m,n+1) + u_2(m,n)] + \Delta t\,\tfrac{1}{2}[E_x(m+1,n) - E_x(m,n)]\{C_+^*(n+\tfrac{1}{2})\,\tfrac{1}{2}[u_3(m,n+1) + u_3(m,n)] + D^*(n+\tfrac{1}{2})\}, \tag{B13}$$

$$u_3(m,n+1) = u_3(m,n) + \Delta t C_-(n+\tfrac{1}{2})\,\tfrac{1}{2}[E_x(m+1,n) - E_x(m,n)]\tfrac{1}{2}[u_1(m,n+1) + u_1(m,n)] + \Delta t C_-^*(n+\tfrac{1}{2})\,\tfrac{1}{2}[E_x(m+1,n) - E_x(m,n)]\tfrac{1}{2}[u_2(m,n+1) + u_2(m,n)]. \tag{B14}$$

The complex CF-FDTD algorithm successfully reproduces the results of the CF-FDTD algorithm for real functions (Appendix A) when simulations were performed with real line shape functions. Their equivalence in this special case can also be verified via substitution of $g^*(t)=g(t)$ into Eqs. (B11)–(B14) and redefinition of the elements of the vector describing the density matrix.

[1] R. G. Brewer and R. L. Shoemaker, Phys. Rev. Lett. **27**, 631 (1971).
[2] R. G. Brewer and R. L. Shoemaker, Phys. Rev. A **6**, 2001 (1972).
[3] S. L. McCall and E. L. Hahn, Phys. Rev. Lett. **21**, 908 (1967).
[4] N. A. Kurnit, I. D. Abella, and S. R. Hartmann, Phys. Rev. Lett. **13**, 567 (1964).
[5] I. D. Abella, N. A. Kurnit, and S. R. Hartmann, Phys. Rev. **141**, 391 (1966).
[6] L. Allen J. H. Eberly, *Optical Resonance and Two-Level Atoms* (Wiley, New York, 1975).
[7] S. Mukamel, *Principles of Nonlinear Optical Spectroscopy* (Oxford University Press, New York, 1995).
[8] T. Joo, Y. Jia, J.-Y. Yu, M. J. Lang, and G. R. Fleming, J. Chem. Phys. **104**, 6089 (1996).
[9] W. P. de Boeij, M. S. Pshenichnikov, and D. A. Wiersma, Annu. Rev. Phys. Chem. **49**, 99 (1998).
[10] L. J. Kaufman, J. Heo, L. D. Ziegler, and G. R. Fleming, Phys. Rev. Lett. **88**, 207402 (2002).
[11] K. J. Kubarych, C. J. Milne, S. Lin, V. Astinov, and R. J. D. Miller, J. Chem. Phys. **116**, 2016 (2002).
[12] A. Albrecht Ferro, J. D. Hybl, and D. M. Jonas, J. Chem. Phys. **114**, 4649 (2001).
[13] Y.-H. Liau, S. Egusa, and N. F. Scherer, Opt. Lett. **27**, 857 (2002).
[14] M. C. Beard and C. A. Schmuttenmaer, J. Chem. Phys. **114**, 2903 (2001).
[15] O. D. Muecke, T. Tritschler, M. Wegener, U. Morgner, and F. X. Kärtner, Phys. Rev. Lett. **87**, 057401 (2001).
[16] S. Hughes, Phys. Rev. A **62**, 055401 (2000).
[17] M. Bonn, S. Woutersen, and H. J. Bakker, Opt. Commun. **147**, 138 (1998).
[18] D. S. Kim, J. Shah, D. A. B. Miller, T. C. Damen, W. Schaefer, and L. Pfeiffer, Phys. Rev. B **48**, 17902 (1993).
[19] D. S. Kim, J. Shah, D. A. B. Miller, T. C. Damen, A. Vinattieri, W. Schaeffer, and L. N. Pfeiffer, Phys. Rev. B **50**, 18240 (1994).
[20] J. A. Gruetzmacher and N. F. Scherer, Rev. Sci. Instrum. **73**, 2227 (2002).
[21] M. D. Crisp, Phys. Rev. A **1**, 1604 (1970).
[22] U. van Bürck, Hyperfine Interact. **123/124**, 483 (1999).
[23] F. C. Spano and W. S. Warren, J. Chem. Phys. **93**, 1546 (1990).
[24] R. W. Olson, H. W. H. Lee, F. G. Patterson, and M. D. Fayer, J. Chem. Phys. **76**, 31 (1982).
[25] H.-J. Hartmann and A. Laubereau, J. Chem. Phys. **80**, 4663 (1984).
[26] R. Laenen and A. Laubereau, Opt. Commun. **101**, 43 (1993).
[27] S. Yeremenko, M. S. Pshenichnikov, and D. A. Wiersma, Chem. Phys. Lett. **369**, 107 (2003).
[28] A. Laubereau and W. Kaiser, Rev. Mod. Phys. **50**, 607 (1978).
[29] A. Taflove and S. C. Hagness, *Computational Electrodynamics: The Finite-Difference Time-Domain Method*, 2nd ed. (Artech House, Norwood, MA, 2000).
[30] R. J. Luebbers and K. S. Kunz, *The Finite Difference Time Domain Method for Electromagnetics* (CRC, Boca Raton, 1993).
[31] S. Mukamel, Chem. Phys. **37**, 33 (1979).
[32] J. A. Gruetzmacher and N. F. Scherer (in preparation).
[33] As implied by the form of Eqs. (1) and (2), all equations herein will be expressed in the mks (SI) system of units.
[34] R. J. Luebbers, F. P. Hunsberger, K. S. Kunz, R. B. Standler, and M. Schneider, IEEE Trans. Electromagn. Compat. **32**, 222 (1990).
[35] D. F. Kelly and R. J. Luebbers, IEEE Trans. Antennas Propag. **44**, 792 (1996).
[36] R. M. Joseph, S. C. Hagness, and A. Taflove, Opt. Lett. **16**, 1412 (1991).
[37] A. V. Tarasishin, S. A. Magnitskii, and A. M. Zheltikov, Opt. Commun. **193**, 187 (2001).
[38] A. V. Tarasishin, S. A. Magnitskii, V. A. Shuvaev, and A. M. Zheltikov, Opt. Express **8**, 452 (2001).
[39] S. Hughes, Phys. Rev. Lett. **81**, 3363 (1998).
[40] R. W. Ziolkowski, J. M. Arnold, and D. M. Gogny, Phys. Rev. A **52**, 3082 (1995).
[41] J. Xiao, Z. Wang, and Z. Xu, Phys. Rev. A **65**, 031402(R) (2002); V. P. Kalosha and J. Herrmann, Phys. Rev Lett. **83**, 544 (1999).
[42] J. A. Gruetzmacher and N. F. Scherer, Opt. Lett. **28**, 573 (2003).
[43] R. G. Gordon, J. Chem. Phys. **43**, 1301 (1968).
[44] R. Kubo, in *Fluctuation, Relaxation, and Resonance in Magnetic Systems* (Oliver and Boyd, New York, 1962).
[45] S. Mukamel, I. Oppenheim, and J. Ross, Phys. Rev. A **17**, 1988 (1978).
[46] S. Linden, H. Giessen, and J. Kuhl, Phys. Status Solidi B **206**, 119 (1998).
[47] J. Stenger, D. Madsen, P. Hamm, E. T. J. Nibbering, and T. Elsaesser, Phys. Rev. Lett. **87**, 027401 (2001).
[48] J. Stenger, D. Madsen, P. Hamm, E. T. J. Nibbering, and T. Elsaesser, J. Phys. Chem. A **106**, 2341 (2002).
[49] S. Woutersen and H. J. Bakker, Phys. Rev. Lett. **83**, 2077 (1999).
[50] H. R. Wyss and M. Falk, Can. J. Chem. **48**, 607 (1970).
[51] J. E. Bertie, M. Khalique Ahmed, and H. H. Eysel, J. Phys. Chem. **93**, 2210 (1989).
[52] G. M. Gale, G. Gallot, F. Hache, N. Lascoux, S. Bratos, and J.-C. Leicknam, Phys. Rev. Lett. **82**, 1068 (1999).
[53] G. M. Gale, G. Gallot, and N. Lascoux, Chem. Phys. Lett. **311**, 123 (1999).
[54] R. M. Joseph, P. M. Goorjian, and A. Taflove, Opt. Lett. **18**, 491 (1993).
[55] R. W. Ziolkowski, IEEE Trans. Antennas Propag. **45**, 375 (1997).
[56] R. Laenen, C. Rauscher, and A. Laubereau, Phys. Rev. Lett. **80**, 2622 (1998).
[57] R. Laenen, C. Rauscher, and A. Laubereau, J. Phys. Chem. B **102**, 9304 (1998).
[58] H.-K. Nienhuys, S. Woutersen, R. A. van Santen, and H. J. Bakker, J. Chem. Phys. **111**, 1494 (1999).
[59] G. Slavcheva, J. M. Arnold, I. Wallace, and R. W. Ziolkowski, Phys. Rev. A **66**, 063418 (2002).
[60] K. S. Yee, IEEE Trans. Antennas Propag. **14**, 302 (1966).